Bioconjugate Chemistry

Article

pubs.acs.org/bc

Novel ^{18}F Labeling Strategy for Polyester-Based NPs for in Vivo PET-CT Imaging

Primiano Pio Di Mauro,[†,‡] Vanessa Gómez-Vallejo,[∥] Zuriñe Baz Maldonado,[§] Jordi Llop Roig,*[,§] and Salvador Borrós*[,†,‡]

[†]Sagetis-Biotech, 08017 Barcelona, Spain

[‡]Grup d'Enginyeria de Materials (GEMAT), Institut Quimic de Sarria, Universidad Ramon Llull, 08017 Barcelona, Spain

[§]Radiochemistry and Nuclear imaging and [∥]Radiochemistry Department, CIC biomaGUNE, 20009 San Sebastian, Spain

Supporting Information

ABSTRACT: Drug-loaded nanocarriers and nanoparticulate systems used for drug release require a careful in vivo evaluation in terms of physicochemical and pharmacokinetic properties. Nuclear imaging techniques such as positron emission tomography (PET) are ideal and noninvasive tools to investigate the biodistribution and biological fate of the nanostructures, but the incorporation of a positron emitter is required. Here we describe a novel approach for the ^{18}F-radiolabeling of polyester-based nanoparticles. Our approach relies on the preparation of the radiolabeled active agent 4-[^{18}F]fluorobenzyl-2-bromoacetamide ([^{18}F]FBBA), which is subsequently coupled to block copolymers under mild conditions. The labeled block copolymers are ultimately incorporated as constituent elements of the NPs by using a modified nano coprecipitation method. This strategy has been applied in the current work to the preparation of peptide-functionalized NPs with potential applications in drug delivery. According to the measurements of particle size and zeta potential, the radiolabeling process did not result in a statistically significant alteration of the physicochemical properties of the NPs. Moreover, radiochemical stability studies showed no detachment of the radioactivity from NPs even at 12 h after preparation. The radiolabeled NPs enabled the in vivo quantification of the biodistribution data in rats using a combination of imaging techniques, namely, PET and computerized tomography (CT). Low accumulation of the nanoparticles in the liver and their elimination mainly via urine was found. The different biodistribution pattern obtained for the "free" radiolabeled polymer suggests chemical and radiochemical integrity of the NPs under investigation. The strategy reported here may be applied to any polymeric NPs containing polymers bearing a nucleophile, and hence our novel strategy may find application for the in vivo and noninvasive investigation of a wide range of NPs.

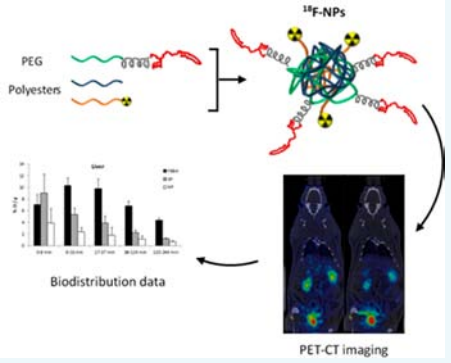

INTRODUCTION

Nanomaterials (NMs) can be broadly classified as organic/polymeric, carbon based, inorganic, and hybrid. Inorganic NMs can have very different surface-to-volume ratios and shapes[1,2] and are ubiquitously utilized as food or paint additives,[3,4] in the construction and semiconductor industries,[5,6] in cosmetic applications,[7] and in many other industrial and societal sectors. Carbon based NMs formed by carbon in sp2 conformation have recently gained significant attention for their potential applications in a varied range of industries such as spintronics[8,9] and sensor development.[10,11] Organic/polymeric NMs are frequently applied in nanomedicine.[12] Finally, hybrid NMs combine materials of different natures, e.g., as core/shell NMs or hierarchical structures, leading thus to a limitless number of scenarios in terms of chemical composition, potential complexity of the NMs, and their applications.

Among NMs, polymer based nanoparticles (PNPs) have been proposed as suitable drug delivery vehicles. Since many drugs and therapeutic agents have poor pharmacokinetic properties, their entrapment into PNPs can be anticipated as a valuable alternative to enhance their therapeutic worth by improving their bioavailability, solubility in physiological environment, or circulation time.[13,14] Additionally, carrier NPs can enable delayed drug release and improve selective accumulation in specific tissues, by attachment of specific targeting moieties on the NPs surface.

Nanocarriers designed for the selective delivery of drugs to specific tissues or organs after systemic administration require long circulation times in the bloodstream, in order to reach the targeted organ or tissue before clearance or degradation occurs.[15−18] This is not likely to happen if the carrier is taken up by the mononuclear phagocyte system (MPS, also called reticuloendothelial system or RES) immediately after intravenous administration, or if rapid renal excretion occurs. Similar considerations are needed for nanosystems meant to be a circulating reservoir for sustained release of therapeutic

Received: January 18, 2015
Revised: February 22, 2015
Published: February 24, 2015

DOI: 10.1021/acs.bioconjchem.5b00040
Bioconjugate Chem. 2015, 26, 582−592

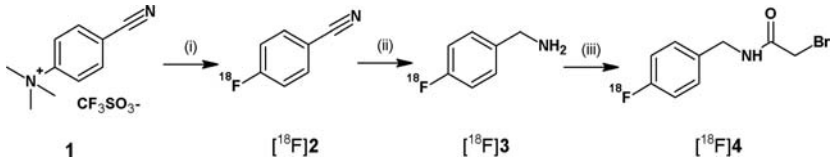

Figure 1. Scheme of the reaction for the preparation of [^{18}F]FBBA ([^{18}F]**4**); (i) azeotropically dried [^{18}F]F$^-$, K_2CO_3, $K_{2.2.2.}$, MeCN, 130 °C, 10 min; (ii) 0.1 M $LiAlH_4$, 2 min, 120 °C; (iii) bromoacetyl bromide in CH_2Cl_2, 2 min, RT.

cargoes. Hence, investigation of the pharmacokinetic properties of PNPs with biomedical applications is of paramount importance.

Different approaches can be used to investigate the pharmacokinetic properties of PNPs. Invasive visualization methods such as optical or electron microscopies are often employed. Alternatively, in vivo imaging techniques such as positron emission tomography (PET), single photon emission computerized tomography (SPECT), magnetic resonance imaging (MRI), or fluorescence tomography can also be applied. Among them, PET offers unparalleled in vivo sensitivity; in addition, due to the high penetration capacity of the high-energy (511 keV) γ rays resulting from positron annihilation, it can be applied to both small and large animal species as well as humans. Hence, PET represents an ideal tool to investigate, in vivo and noninvasively, the biological fate of NPs, including stability in biological environments (stealthiness), pharmacokinetics, and specific organ uptake.[19]

The investigation of the pharmacokinetic properties of NPs using PET requires the incorporation of a positron emitter in the NP (radiolabeling). To date, different PNP-radiolabeling strategies have been developed, with attachment of a radiometal (e.g., ^{68}Ga or ^{64}Cu)[20,21] by means of a bifunctional chelator (BFC) the most commonly used. Despite being very useful in a wide variety of scenarios, attachment of a radionuclide using BFCs has several drawbacks. First, formation of the chelator−radiometal complex may be hampered if the chelators (which are usually attached to the NPs during preparation) are sterically hindered or not accessible. Second, the presence of nonradioactive metals with the capacity to form complexes with the chelator during the entire production process may compromise the radiochemical yields and the specific radioactivity of the resulting radiolabeled PNPs. Finally, release of the radiometal or transchelation due to the presence of certain proteins during in vivo investigations may lead to completely wrong conclusions, as the presence of the free radionuclide might be mistakenly interpreted as a signature of the PNP presence. This limitation can be circumvented by using appropriate chelators with low dissociation constants; previous knowledge regarding the biodistribution pattern for the free radionuclide may also help in interpretation of the results.

One alternative to the use of radiometals consists of radiolabeling the NPs with ^{18}F, a relatively long-half-life positron emitter ($T_{1/2}$ = 109.7 min), which can be produced as [^{18}F]F$^-$ in the GBq scale in all biomedical cyclotrons. Unfortunately, direct labeling with [^{18}F]F$^-$ requires harsh conditions (for example, high temperature and water-free organic solvent), and long reaction times;[22] alternatively, indirect labeling methods can be used. In these, a radiolabeled prosthetic group is prepared in a first step and subsequently coupled to the molecule of interest, usually under mild conditions. This strategy has been applied to the preparation of radiolabeled NPs;[23,24] of note, the presence of a reactive group on the surface of the NPs able to react with the labeled prosthetic group is required, and hence this strategy cannot be directly translated to certain types of polymeric NPs. The development of alternative synthetic routes is thus particularly convenient.

Very recently, we reported the preparation of Paclitaxel-loaded PNPs using a modified nanoprecipitation method.[25] In this work, and following a similar synthetic strategy, we present an unprecedented strategy for the preparation of analogous radiolabeled PNPs. Our method relies on radiolabeling block copolymers using the labeling agent 4-[^{18}F]fluorobenzyl-2-bromoacetamide ([^{18}F]FBBA). These block copolymers are ultimately incorporated in the PNPs as constituent elements. The strategy has been applied to the preparation of radiolabeled, peptide-functionalized PNPs with potential applications in drug delivery. Finally, quantitative biodistribution data was obtained in vivo after intravenous administration in rodents using a combination of imaging techniques. The strategy reported here relies in the condensation of the labeling agent [^{18}F]FBBA with a polymer containing a nucleophile, and subsequent utilization of the labeled polymer for the preparation of radiolabeled NPs. Hence, our approach may find application in the preparation of a wide range of radiolabeled polymeric NPs, and become thus an interesting tool for the evaluation of the pharmacokinetic properties of newly developed PNPs.

RESULTS AND DISCUSSION

Synthesis and Characterization of [^{18}F]FBBA and ^{18}F-Labeled Polymers. The labeled active agent [^{18}F]FBBA was synthesized following a well established three-step procedure (Figure 1).[26] First, 4-[^{18}F]fluorobenzonitrile ([^{18}F]**2**) was prepared by reaction of 4-cyano-*N*,*N*,*N*-trimethylanilinium trifluoromethanesulfonate (**1**) with [^{18}F]F$^-$. After purification using solid phase extraction and water removal using Na_2SO_4 and molecular sieves, the cyano group in [^{18}F]**2** was efficiently reduced with $LiAlH_4$ to yield [^{18}F]**3**, which was further reacted with bromoacetyl bromide to yield [^{18}F]**4**. After purification using HPLC, the presence of the desired labeled species was confirmed by HPLC and coelution with reference standard (Figure 2). Radiochemical yields similar to those previously reported in the literature (12%, decay corrected; total synthesis time approximately 90 min including purification) were achieved. It is worth mentioning that an alternative methodology for the preparation of [^{18}F]FBBA with overall decay corrected radiochemical yield of 75% (total synthesis time: 1 h) has been reported.[27] In this work, the reduction step was based on borohydride exchange resin in substitution of $LiAlH_4$. This methodology was not implemented in our lab; however, its utilization would lead to higher overall radiochemical yields in the preparation of labeled polymers and NPs (vide infra).

The synthesis of radiolabeled polymers using prelabeled prosthetic groups has been previously reported in the literature. For example, Herth and co-workers[28] reported the preparation of labeled *N*-(2-hydroxypropyl)-methacrylamide (HPMA)-

DOI: 10.1021/acs.bioconjchem.5b00040
Bioconjugate Chem. 2015, 26, 582−592

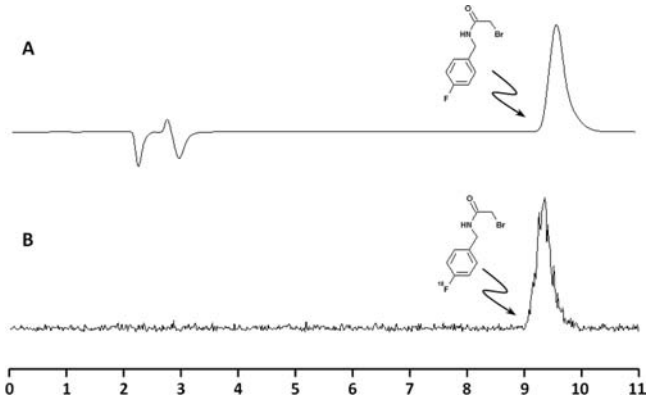

Figure 2. HPLC chromatograms corresponding to (A) FBBA (reference standard solution, UV detector) and (B) [^{18}F]FBBA (purified fraction, radiometric detector).

based polymers by aminolyzing functional reactive ester polymers, which were subsequently reacted with the labeling synthon 2-[^{18}F]fluoroethyl-1-tosylate ([^{18}F]FETos). These polymers showed excellent radiochemical stability and were used to perform biodistribution studies in healthy and tumor-bearing animals.[29,30]

Following a similar strategy to those previously reported, we approached the preparation of ^{18}F-labeled PEG-thiol-acids by condensation of [^{18}F]**4** with the corresponding α-thio-ω-carboxy poly(ethylene glycol) (MWs of 458.6 and 3300 Da). These experiments were conducted to have a proof of principle of the feasibility of the condensation reaction, to be translated later on to the radiolabeling of block copolymers P and 3P (vide infra). The coupling reaction (see Figure 3 for PEG-thiol-

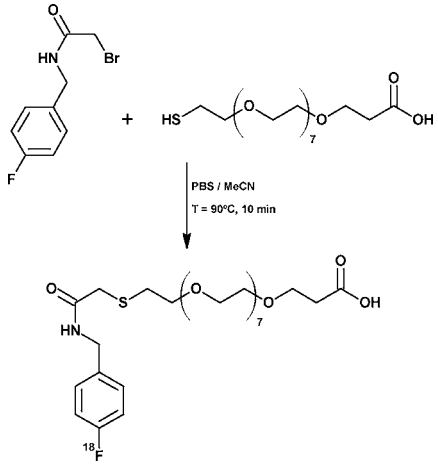

Figure 3. Synthesis of [^{18}F]-FBBA-PEG-thiol-acid by the condensation of [^{18}F]FBBA with PEG-thiol-acid with Mw 458.6 Da.

acid with MW = 458.6 Da) was optimized by using different temperatures and reaction times, and the radiochemical conversion (RCC) was determined by direct integration of the radiometric chromatographic profiles at different reaction times. For the low MW PEG-thiol-acid, RCC values at 90 °C reached a plateau (>90% RCC) at t > 10 min. A similar kinetic profile was also observed at T = 70 °C, although lower conversion values (<85%) could be achieved and the plateau was slightly delayed (t > 20 min) (Figure S1). Very similar results were obtained for the higher MW PEG-thiol-acid. A plateau was reached at t > 10 min at 90 °C, with RCC values in the range 84−87%. These values dropped to 71−78% at T = 70 °C (Figure S2).

Large scale synthesis under optimal conditions resulted in overall radiochemical yields (referred to [^{18}F]FBBA) of 51 ± 7% (uncorrected) after purification (see Figure S3 for an example of chromatographic profiles). UPLC-ESI/MS and MALDI-TOF-MS analysis of the collected fractions confirmed the presence of the condensation products. Major peaks at m/z = 624.3 (M + H^+) and 641.3 (M + NH_4^+) were detected for low MW PEG-thiol acid (Figure S4) and m/z = 1691.26 for high MW PEG-thiol acid, the latter corresponding approximately to half of the molecular weight of the condensation product (Figure S5).

The first and second strategies used for the preparation of radiolabeled NPs (vide infra) required the preparation of radiolabeled block copolymers P and 3P (namely, [^{18}F]P and [^{18}F]3P). Incorporation of the labeled active agent [^{18}F]FBBA into block copolymers P and 3P was carried out following the chemical reaction schematized in Figures 4 and 5, respectively. Radiochemical conversion values of 52% and 65% were achieved for polymer P at 90 and 120 °C, respectively. However, at 120 °C the reaction occurred faster, reaching a plateau after 30 min. The plateau was reached only after 120 min when the reaction was conducted at 90 °C (Figure S6). For 3P block copolymer, radiochemical conversion was approximately 60% after 1 h when the reaction was carried out at 120 °C (Figure S7). After purification by HPLC, [^{18}F]P and [^{18}F]3P could be obtained in overall decay-corrected radiochemical yields of 17 ± 4% and 27 ± 7%, respectively, referring to the starting amount of [^{18}F]FBBA (total synthesis time starting from [^{18}F]FBBA: 50 min for [^{18}F]P and 80 in for [^{18}F]3P).

Synthesis and Characterization of [^{18}F]-Labeled NPs. In a previous work we have developed a peptide-targeted nano system able to modulate and control the release of PTX across an in vitro BBB model based on human glioma cells (results pending from publication). In continuation of this previous work, we selected here AGBBB015F (15F) as the targeting peptide. 15F was introduced in 2007 by Demeule and co-workers,[31] and belongs to a family of peptides named Angiopeps, which were derived from the Kunitz domain of aprotinin. Angiopeps are known to be able to pass through the BBB via a mechanism which involves the LDLR (low density lipoprotein receptor).

Here, by modifying the nano coprecipitation method, ^{18}F-labeled/peptide-functionalized NPs were obtained following three different methods as specified in the Experimental Procedures (see Figure 6 and Synthesis of Block Copolymer 2P). These three strategies resulted in values of radiolabeling efficiency ranging from 5% to 14%, related to the amount of starting radiolabeled polymer (strategies 1 and 2) or starting amount of [^{18}F]FBBA (strategy 3) (Table 1). Considering the radiochemical yields of all individual steps, this results in overall decay-corrected radiochemical yields of approximately 0.1%, 0.45%, and 1.2% (referred to [^{18}F]F^-) in overall preparation times of 200, 230, and 150 min for strategies 1−3, respectively. In other words, with a starting [^{18}F]F^- activity of 37GBq (which is easily achieved in commercially available cyclotrons), the final amount of radioactivity in the NPs is 10, 39, and 170 MBq, respectively, which is low but still sufficient to approach in vivo experiments.

According to the measurements of particle size and zeta potential, the incorporation of the radiolabel did not result in

DOI: 10.1021/acs.bioconjchem.5b00040
Bioconjugate Chem. 2015, 26, 582−592

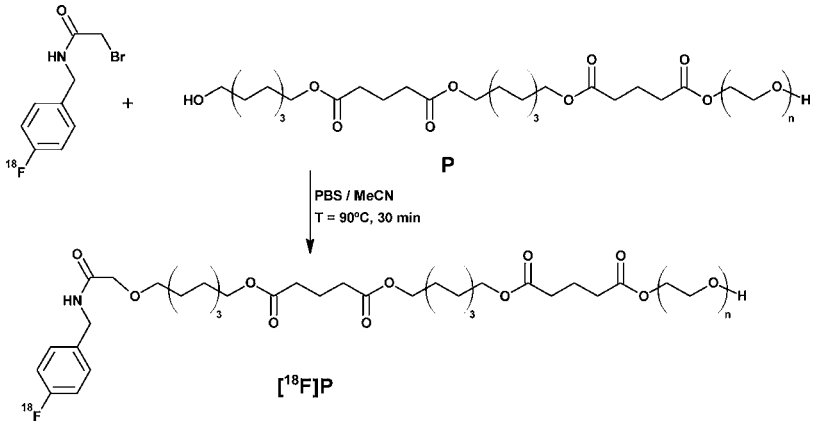

Figure 4. Synthesis of [^{18}F]FBBA-P block copolymer ([^{18}F]P).

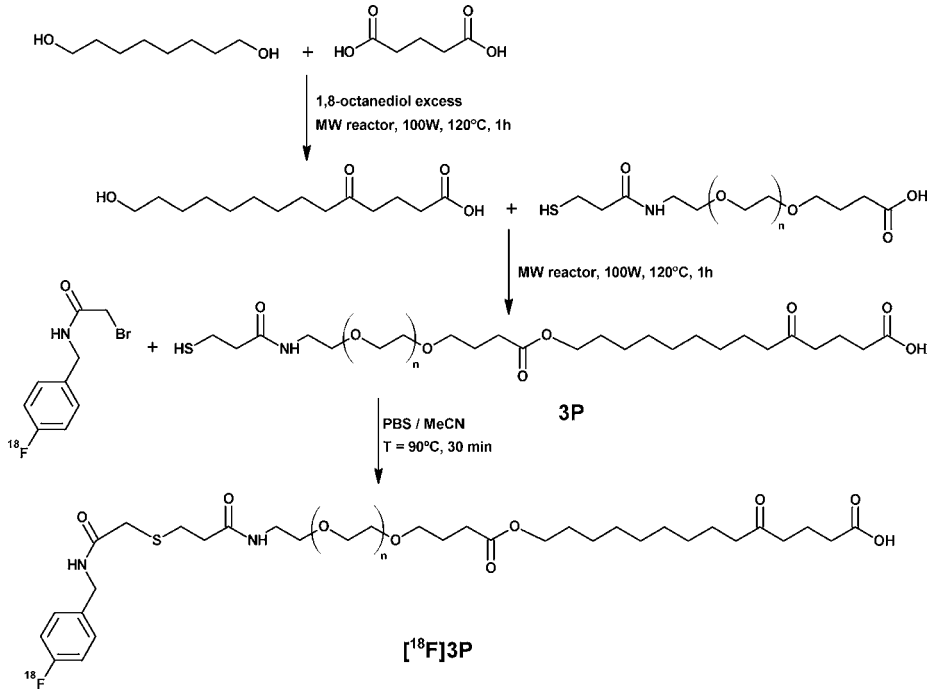

Figure 5. Synthesis of [^{18}F]FBBA-3P block copolymer ([^{18}F]3P).

statistically significant alteration of the physicochemical properties of the resulting NPs. All the formulations exhibited average diameters in the desired range (below 200 nm) with a narrow size distribution (polydispersity ranging from 0.05 to 0.282) (Table 1). Moreover, all formulations exhibited a net negative charge with zeta-potential values approximately of −30 mV.

To confirm that the bioactivity of the coupled peptide is retained after incorporation into the PNPs, a transendothelial transport experiments in an in vitro BBB model was performed (see Supporting Information Figure S8).

Radiochemical stability studies showed no detachment of the radioactivity for NPs prepared following strategies 1 and 2 (radiochemical purity >95% after 12 h). Slow detachment of [^{18}F]FBBA was observed at long times for NPs synthesized following strategy 3 (% of radioactivity attached to the NPs: 78 ± 12% at t = 1 h, 64 ± 4% at t = 3 h, 42 ± 8% at t = 12 h). As shown in a previous study,[25] degradation of the NPs may occur during the first days through uniform bulk degradation of the matrix. However, the relatively fast detachment of [^{18}F]FBBA could be attributed to a simple diffusion process through the polymer core matrix, as a result of water penetration.

In Vivo Biodistribution in Rats (PET-CT Imaging). In vivo biodistribution studies using PET imaging were carried out using the labeled NPs prepared according to strategy 2 (this is, using [^{18}F]3P as a labeled precursor). This decision was made based on radiochemical yields during particle preparation (see Table 1) and stability studies. The labeled precursors (namely, [^{18}F]FBBA and [^{18}F]3P) were also investigated as controls. PET dynamic images were acquired after intravenous administration of the labeled species and quantified by drawing volumes of interest (VOIs) on the CT images for selected organs (i.e., kidneys, liver, stomach, and brain).

Figure 7 displays the percentage of injected dose per gram of tissue (%ID/g) obtained after analysis of the PET data. As can be seen, [^{18}F]FBBA showed a high uptake in the brain at short times after administration, followed by a progressive wash-out at t > 16 min. Such high uptake may be due to the hydrophobic character of the molecule. [^{18}F]FBBA also showed significant uptake in the liver (approximately 10%ID/g at 9 min < t < 37

DOI: 10.1021/acs.bioconjchem.5b00040
Bioconjugate Chem. 2015, 26, 582−592

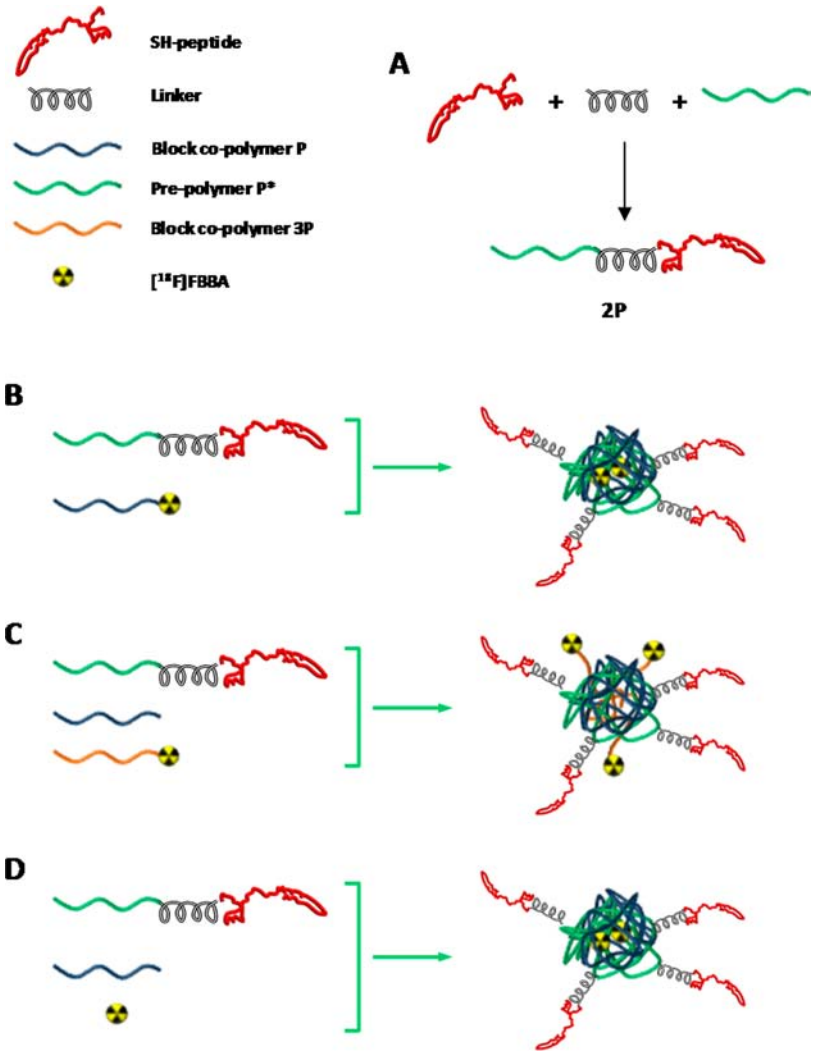

Figure 6. (A) Schematic illustration of the three strategies employed for the fabrication of ^{18}F-labeled and peptide-functionalized-NPs via coprecipitation. Labeled parts are (B) block copolymer P (strategy 1), (C) block copolymer 3P (strategy 2), and (D) entrapped [^{18}F]FBBA (strategy 3).

Table 1. Radiochemical Yields for the Preparation of [^{18}F]FBBA, [^{18}F]polymers, and [^{18}F]NPs, for Each of the Strategies of Preparation of NPs (Radionuclide Anchored to Polymers P and 3P, and Encapsulation of [^{18}F]FBBA)[a]

^{18}F-labeling strategy	DC RCY[b] for [^{18}F]FBBA[c] (time)	DC RCY[b] for [^{18}F]polymer[d] (time)	DC RCY[b] for [^{18}F]NPs[e] (time)	hydrodynamic diameter (nm)[f]
[^{18}F]P	12% (90 min)	17% (50 min)	5% (60 min)	173 ± 13 nm
[^{18}F]3P	12% (90 min)	27% (80 min)	14% (60 min)	185 ± 20 nm
[^{18}F] FBBA	12% (90 min)	NA	10% (60 min)	168 ± 27 nm

[a]Hydrodynamic diameters of the NPs, as determined by DLS, are also included. [b]Decay-corrected radiochemical yield. [c]Referred to [^{18}F]F$^-$. [d]Referred to [^{18}F]FBBA. [e]Referred to [^{18}F]polymer (strategies 1 and 2) or [^{18}F]FBBA (strategy 3). [f]As determined by DLS.

min) and in the stomach, while accumulation in the kidneys was lower than the accumulation observed for [^{18}F]3P and [^{18}F]NPs. This suggests a preferential hepatobiliary elimination pathway in combination with renal excretion. Significant accumulation in the lungs (not shown in Figure 7) was also observed, especially at short times after administration. This accumulation decreased over time, although at long times the presence of radioactivity in the lungs could still be detected (see Figure 8A for PET-CT images).

[^{18}F]3P showed low accumulation in the brain with fast washout and very high accumulation in the kidneys, although uptake in the liver and the stomach was also significant. Again, this suggests elimination via the hepatobiliary system in combination with renal excretion.

Interestingly, labeled NPs showed a low accumulation in the liver and elimination mainly via urine. Accumulation in the liver increased rapidly to reach values around 4%ID/g; these values rapidly decreased at longer times after administration until values close to 1%ID/g were reached. Time−activity curves in the brain and in the kidneys followed a similar pattern to [^{18}F]3P, while lower accumulation was observed in the stomach, with values close to 1%ID/g all over the duration of the study.

Actually, when NPs are administered, a variety of plasma proteins (e.g., opsonins) tend to bind to their surfaces. The conjugates can then be recognized by the MPS and internalized in macrophages, leading to a significant loss of NPs from circulation. The decoration of the NPs with a PEG layer prevents opsonization and sequestration by the MPS, resulting

DOI: 10.1021/acs.bioconjchem.5b00040
Bioconjugate Chem. 2015, 26, 582−592

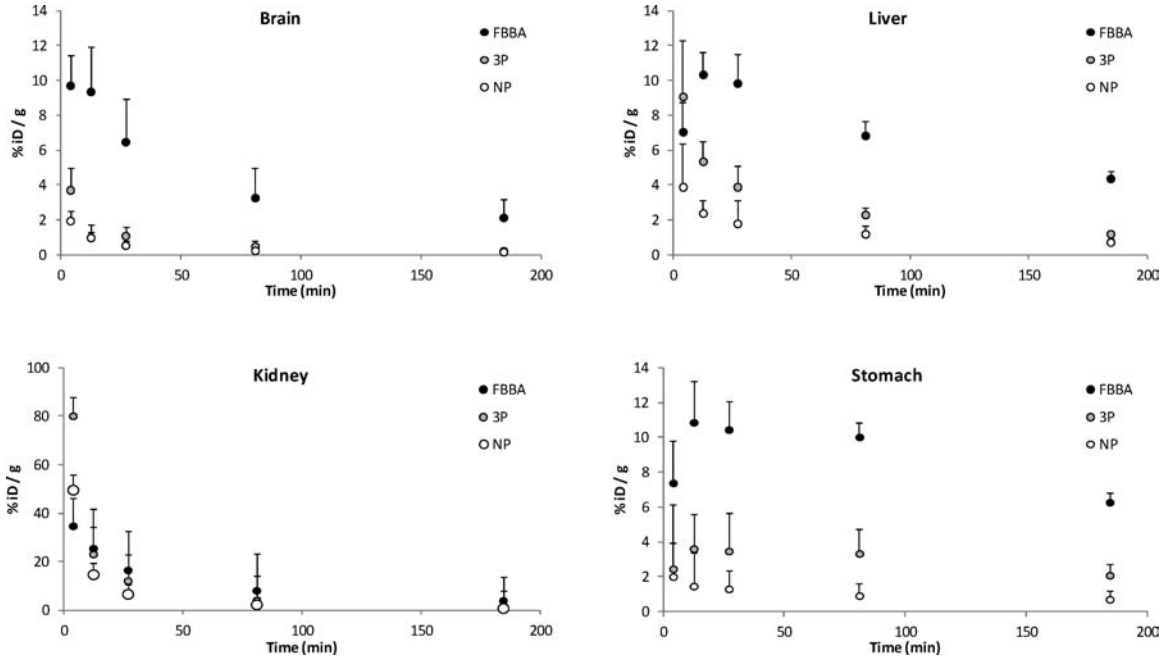

Figure 7. Accumulation of [^{18}F]FBBA (labeled FBBA), [^{18}F]3P (3P), and ^{18}F-labeled NPs (NP) in brain, liver, kidneys, and stomach, expressed as percentage of injected dose (%ID) per gram of organ (mean ± standard deviation, n = 3) at different time points after intravenous administration.

in prolonged blood circulation.[32,33] Hence, our results are in good agreement with the fact that renal excretion of the NPs becomes the preferred route when the NPs are surface-functionalized with PEG; despite the negative superficial charge of the developed peptide-functionalized-NPs, which favors the interaction with the MPS, opsonization and consequently liver accumulation were clearly avoided thanks to stealthy behavior awarded to our nanoparticulate system. The low accumulation in the liver should also prevent hepatotoxicity, which might be a consequence of high liver uptake.[34]

Contrary to NPs, a marked initial renal uptake for [^{18}F]3P block copolymer was observed. These results confirm that low molecular weight block copolymers have a major tendency to be eliminated via urine, contrary to larger molecules or NPs.[34] Of note, the differences in the uptake values obtained for [^{18}F]3P and [^{18}F]NPs suggest the chemical and radiochemical stability of the NPs in vivo, at least during the duration of the study. As shown in Figures 7 and 8, a low accumulation of NPs was observed in the brain despite the presence of the peptide. The low uptake observed at short times after administration might be due to the contribution of the presence of labeled NPs in the blood, and hence animal sacrifice, organ removal, and subsequent determination of the amount of radioactivity using a gamma counter may provide more accurate information about the real concentration of NPs in the brain. However, due to invasiveness of the technique, different animals have to be utilized to obtain uptake values at different time points after administration.

It is worth mentioning that the residence time of the NPs in the body is longer than the time-window in which images can be acquired (up to 8−10 h), due to the relatively short half-life of ^{18}F. In order to obtain data at longer times after administration, different labeling strategies using alternative radioisotopes would be required. A similar labeling strategy can be envisaged by using radioiodinated prosthetic groups bearing bromoacetamide, such as *N*-(4-iodobenzyl)-2-bromoacetamide.[35] In this case, the positron emitter ^{124}I ($T_{1/2}$ = 4.18 days) or the gamma emitter ^{123}I ($T_{1/2}$ = 13.22 h) might be used, enabling the acquisition of images at longer times after administration using PET or SPECT, respectively. If SPECT is used, lower resolution images are obtained and absolute quantification is more challenging. However, qualitative information about the biodistribution pattern and biological fate of the NPs may be obtained.

Interestingly, the synthetic route proposed here requires harsh conditions only for the preparation of the labeling agent ([^{18}F]FBBA) and subsequent formation of the labeled polymers. However, preparation of the NPs takes place under mild conditions. Hence, despite the inconvenience where the label is incorporated in the first step of the process, with the consequent decrease in radiochemical yields and potential increase in dose exposure, NPs with functionalities sensitive to temperature or pH can be prepared. Hence, this is a valid alternative when the NPs to be labeled do not have functionalities suitable for the attachment of radiolabeled tags, or when the addition of chelators for subsequent incorporation of radiometals is not feasible or convenient.

CONCLUSIONS

This work describes a novel approach for the radiolabeling of PNPs and subsequent utilization for the in vivo determination of the biodistribution pattern using a combination of imaging techniques, i.e., positron emission tomography (PET) and computerized tomography (CT). These techniques represent an ideal tool for investigations of pharmacological profiles of new nanosystems. The labeling approach is based on radiolabeling one of the precursor polymers, which is finally integrated in the NP using a nanoprecipitation method. Radiolabeled NPs showed values of size and zeta potential equivalent to those of the unlabeled analogues, within the experimental error. The labeled NPs enabled the quantification of the biodistribution data in rats up to 4 h after intravenous administration. PET images show low accumulation in the liver and elimination mainly via urine. The different biodistribution

DOI: 10.1021/acs.bioconjchem.5b00040
Bioconjugate Chem. 2015, 26, 582−592

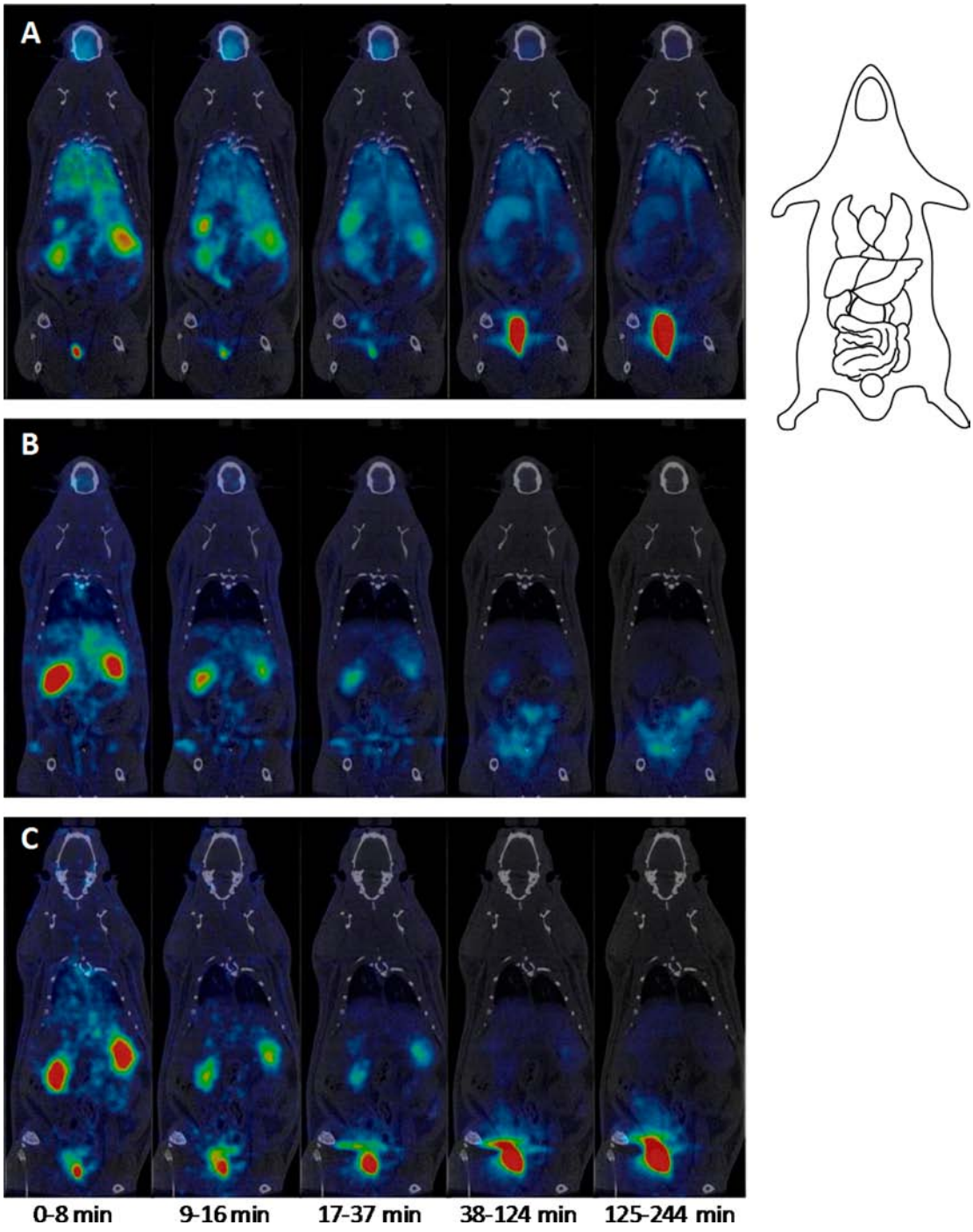

Figure 8. PET images (maximum intensity projections) for [^{18}F]FBBA (A), [^{18}F]3P (B), and [^{18}F]NPs (C) at different time points after administration. Frames within each time gap have been averaged to create the images displayed. Computerized tomography (CT) images were adjusted along the *Y* axis for an appropriate fitting with the tracer distribution image.The intensity of the PET images was adjusted by normalizing with respect to injected dose.

pattern obtained for the "free" radiolabeled polymer ([^{18}F]3P) suggest chemical and radiochemical integrity of the NPs under investigation. The strategy reported here might be applied to the preparation of other radiolabeled polymeric NPs, in order to determine their pharmacokinetic properties and evaluate their potential therapeutic capabilities.

■ EXPERIMENTAL PROCEDURES

The experimental part of this work was carried out in the Molecular and Functional Imaging Facility of CIC biomaGUNE. 1,8-Octanediol (98%), 2,2′-dithiodipyridine (≥97%), and polyethylene glycol (PEG, Mw 1.5 kDa) were purchased from Sigma (Sigma−Aldrich, USA). Glutaric acid (99%) was obtained from Alfa Aesar (USA). AGBBB015F (CGGK-TFFYGGSRGKRNNFKTEEY)) peptide, fluorescently labeled with carboxyfluorescein, was synthesized by Innovagen AB (Sweden). PEG Thiol acids, α-thio-ω-carboxy poly(ethylene glycol) (MW 458.6 and 3300 Da) were supplied by Iris Biotech GmbH (Germany). Ultrapure water (Type I water, ISO 3696) was obtained from a Milli-Q system (Merck Millipore). All

DOI: 10.1021/acs.bioconjchem.5b00040
Bioconjugate Chem. 2015, 26, 582−592

other chemicals, unless otherwise specified, were of analytical grade and were purchased from Sigma (Sigma−Aldrich, Germany).

Synthesis of the ^{18}F-Labeled Prosthetic Group [^{18}F]FBBA. The prosthetic group 4-[^{18}F]fluorobenzyl-2-bromoacetamide ([^{18}F]FBBA, [^{18}F]**4**, Figure 1) was synthesized following a previously reported methodology[26] with minor modifications. 4-[^{18}F]fluorobenzonitrile ([^{18}F]**2**) was prepared by reaction of 4-cyano-*N*,*N*,*N*-trimethylanilinium trifluoromethanesulfonate (**1**) with [^{18}F]F$^-$ generated by proton irradiation of [^{18}O]H_2O (>98%, Rotem Industries Ltd.); [^{18}F]F$^-$ was first trapped in an anion exchange resin and subsequently eluted with K_2CO_3/H_2O and Kryptofix2.2.2/MeCN. After azeotropic evaporation of the solvent, the dried potassium [^{18}F]fluoride-Kryptofix2.2.2 complex was dissolved in dry DMSO and the resulting solution was reacted with **1** (130 °C, 10 min). The reaction mixture containing [^{18}F]**2** was cooled, diluted with purified water (9 mL), and flushed through a C-18 cartridge (Sep-Pak, Waters). The retained labeled species was eluted with 2.5 mL of THF, dried over Na_2SO_4 and molecular sieve, and reacted with $LiAlH_4$ in THF (120 °C, 2 min) to yield [^{18}F]**3**, which was further reacted with bromoacetyl bromide (solution in CH_2Cl_2). After addition of 2 mL of MeCN/water 1/1, the mixture was purified by high performance liquid chromatography (HPLC) using a VP125/10 Nucleosil 100−7C18 semipreparative column (Macherey-Nagel) as stationary phase and MeCN/water 1/1 as the mobile phase to yield [^{18}F]**4** (retention time = 13 min) in overall yield of 12% (decay corrected). The collected fraction was used without further treatment for subsequent labeling steps. The presence of the desired product was confirmed by HPLC and coelution with reference standard, using an Agilent 1200 Series HPLC system with a multiple wavelength UV detector (λ = 254 nm) and a radiometric detector (Raytest). A RP-C18 column (Eclipse XDB C18, 4.6 × 150 mm, 5 μm particle size) was used as stationary phase and water/MeCN (60/40) was used as the mobile phase at a flow rate of 1 mL/min (retention time = 9.5 min, injected volume = 20 μL).

Synthesis of ^{18}F-Labeled PEG-Thiol-Acids. The preparation of ^{18}F-labeled PEG-thiol-acids was carried out by condensation of [^{18}F]**4** with the corresponding α-thio-ω-carboxy poly(ethylene glycol). These experiments were conducted for a proof of principle of the feasibility of the condensation reaction, to be translated later on to the radiolabeling of block copolymers P and 3P (vide infra). Experimentally, a 1 mg/mL solution of PEG-thiol-acid in 1:1 (v/v) phosphate buffer saline and acetonitrile (total volume = 250 μL) was mixed with a solution of [^{18}F]FBBA in water/MeCN (1/1, 250 μL). Two different PEG-thiol-acids with molecular weights of 458.6 (Figure 3) and 3300 Da were used, and experimental conditions were optimized (T = 70−90 °C, t = 10−30 min) in both cases. The radiochemical conversion (RCC) was determined by radio-HPLC, using the same experimental conditions as above.

Large scale syntheses were carried out using the optimal reaction conditions (T = 90 °C, t = 10 min); the radiolabeled species were purified by HPLC under analytical conditions described above using a 500 μL injection loop. The fractions containing the pure labeled polymers were collected, allowed to completely decay, and the identity of the labeled species was confirmed by UPLC/ESI-MS (low MW PEG-thiol-acid) or MALDI-TOF-MS (high MW PEG-thiol-acid). UPLC-MS analyses were performed using an AQUITY UPLC separation module coupled to a LCT TOF Premier XE mass spectrometer (Waters, Manchester, UK). An Acquity BEH C18 column (1.7 μm, 5 mm, 2.1 mm) was used as the stationary phase. The elution buffers were A (water and 0.1% formic acid) and B (methanol and 0.1% formic acid). The column was eluted with a gradient: t = 0 min, 95% A, 5% B; t = 0.5 min, 95% A, 5% B; t = 7.5 min, 1% A, 99% B; t = 10 min, 1% A, 99% B. Total run was 10 min, injection volume was 5 μL, and the flow rate 300 μL/min. The detection was carried out in negative ion mode, monitoring the most abundant isotope peaks from the mass spectra. For MALDI-TOF-MS analyses, the sample preparation was carried out by deposition of 0.5 μL of sample directly onto a pre-spotted Anchorchip (PAC-II 96, Bruker Daltonics) plate that contains α-cyano-hydroxycinnamic acid matrix (HCCA). MALDI-TOF analysis was performed using an UltrafleXtreme III time-of-flight mass spectrometer equipped with a Nd:YAG laser (Smartbeam II, 355 nm, 1 kHz) and controlled by Flex Control 3.3 software (Bruker Daltonics, Bremen, Germany). The acquisitions were carried out in positive-ion reflectron mode at a laser frequency of 500 Hz. The spectrum was acquired at 30% laser fluency and was recorded in the m/z range from 1400 to 2000. The deflector cutoff was set at m/z 1000 and the spectrum resulted from accumulation of 1000 laser shots.

Synthesis of ^{18}F-Labeled P Block Copolymer ([^{18}F]P). The first strategy for the synthesis of radiolabeled NPs required the preparation of radiolabeled block copolymer P, which was prepared by the esterification of 1,8-octanediol with glutaric acid and subsequent reaction with PEG 1500. Glutaric acid (6 g, 45 mmol) and 1,8-octanediol (5.53 g, 37 mmol) were reacted in a microwave reactor (Discovery CEM) at 100 W for 1 h. The reaction was performed under vacuum (100 mbar) with continuous stirring by air-cooling to maintain the temperature constant at 120 °C to form the prepolymer. Subsequently, PEG 1500 was added (1:1 weight ratio with the prepolymer) and the polymerization reaction was conducted in the microwave reactor with the conditions described above (100 W, 1 h) to yield P as a white solid.

For the radiosynthesis of [^{18}F]FBBA-labeled P block copolymer ([^{18}F]P), a 1 mg/mL solution of P in 1:1 (v/v) phosphate buffer saline and acetonitrile (total volume = 250 μL), was mixed with an equal volume of a solution of [^{18}F]FBBA in water/acetonitrile (Figure 4). The reaction was incubated at a predetermined temperature and the radiochemical conversion was monitored at different times from chromatographic profiles (chromatographic conditions described above). Different incubation times (10−180 min) and temperatures (90 and 120 °C) were tested in order to achieve optimal reaction conditions.

Large scale syntheses for in vivo experiments were carried out using the optimal reaction time (30 min) and temperature (120 °C); the radiolabeled species was purified by HPLC under conditions described above, using a 500 μL injection loop.

Synthesis of ^{18}F-Labeled 3P Block Copolymer ([^{18}F]3P). The second strategy for the preparation of radiolabeled NPs (vide infra) required the preparation of a novel block copolymer (3P) labeled with ^{18}F (Figure 5). First, the microwave-assisted production of a prepolymer (P*) was approached by reacting glutaric acid and 1,8-octanediol at a molar ratio of 1:1.2 at 100 W for 1 h. The reaction was performed under vacuum with continuous stirring and air-cooling to maintain the temperature at 120 °C. The resulting prepolymer P*, which contained an excess of 1,8-octanediol,

DOI: 10.1021/acs.bioconjchem.5b00040
Bioconjugate Chem. 2015, 26, 582−592

was reacted with the PEG-thiol-acid (3.3 kDa) to obtain 3P block copolymer. This second reaction was conducted in a microwave reactor under experimental conditions described above (100 W, 1 h), using a 1:1 (w/w) ratio between P* and PEG-thiol-acid. Finally, radiolabeling of 3P was achieved by condensation with [^{18}F]FBBA, under the same experimental conditions used for the preparation of ^{18}F-labeled PEG-thiol-acids.

Synthesis of Block Copolymer 2P. In order to achieve targeted NPs, a block copolymer attached via a linker to peptide AGBBB015F was used during NP preparation. For the preparation of the linker, 2,2′-dithiodipyridine (MW 220.31, 66.4 mg, 2.14 mmol) in THF (5 mL) and AcOH (5 mL) were added to an oven-dried one-necked flask under nitrogen atmosphere. α-Thio-ω-carboxy poly(ethylene glycol) (MW 3317 Da, 500 mg, 1.07 mmol) dissolved in THF was added dropwise and the solution was allowed to stir for 3 days. The product was then precipitated by addition of hexane (100 mL) under low magnetic stirring. The solution was refrigerated overnight at 8−10 °C, and subsequently vortexed and centrifuged (two cycles, 2700 *g*, 15′ and 1300 *g*, 20′). After each cycle the supernatant was removed, the same amount of hexane was added, and a short vortex agitation to redisperse the pellet was performed. Residual solvent was removed under vacuum to yield the product as a yellow solid.

The coupling between cysteine residues present at AGBBB015F and linker was carried out in 5 mL PBS (10 mM, pH 7.4). Linker and peptide (1:1.05 molar ratio) were accurately mixed and the reaction was stirred at 0 °C for 4 h to reach quantitative conversion. The solution was finally lyophilized to yield Peptide-Targeted Linker as a white powder.

Finally, to obtain the block copolymer 2P, a preliminary step for the production of the prepolymer P* was needed. Glutaric acid and 1,8-octanediol (molar ratio of 1:1.2) were reacted under microwave heating at 100 W for 1 h. The prepolymer P*, containing an excess of 1,8-octanediol, was reacted with the linker bearing AGBBB015F in the microwave reactor under identical conditions to those described above and using a ratio 1:1 (w/w) between preformed peptide-targeted linker and prepolymer P*. The resulting targeted block copolymer was obtained as a white solid.

Synthesis and Characterization of [^{18}F]-Labeled/Peptide-Functionalized NPs. The synthesis of ^{18}F-labeled/peptide functionalized NPs was approached following a previously reported nano coprecipitation method,[25] with some modifications. Three different strategies were followed, depending on the labeled species used. In all of them, peptide-functionalized block copolymer 2P (Figure 6A) was used as one of the starting materials. The first strategy (Figure 6B) consisted of dissolving block copolymers [^{18}F]P and 2P at 9:1 (w/w) ratio in 1 mL of acetone to form the diffusing phase. This phase was then added to 20 mL of ultrapure water by means of a syringe controlled by a syringe pump (KD Scientific) under magnetic stirring at room temperature; the needle was positioned directly in the medium and a flow rate of 50 μL/min was used. The resulting suspension was allowed to stir uncovered, in order to allow the evaporation of acetone. The suspension was purified by centrifugation (Hettich Centrifuge, EBA 21, 4000 *g*, 45 min at RT) with ultracentrifugal filters (Amicon Ultra-15, Ultracel membrane with 100 000 MWCO, Millipore, USA). The second strategy (Figure 6C) consisted of dissolving block copolymers P, 2P, and [^{18}F]3P in the organic phase (acetone) at a ratio 8:1:1 (w/w), and following exactly the same experimental procedure. Finally, and taking advantage of the hydrophobic character of the labeled prosthetic group, a third strategy (Figure 6D) consisting of encapsulating [^{18}F]FBBA into the peptide-functionalized NPs was approached. With that aim, the labeled species ([^{18}F]FBBA) was dissolved in the organic phase (acetone, 1 mL) together with the starting polymers (P and 2P), and the solution was added dropwise to the aqueous phase under continuous stirring, following the same experimental procedure.

In all cases, the physicochemical properties (size and zeta potential) of the resulting ^{18}F-labeled/peptide-functionalized NPs were determined after complete decay as described in our previous work.[25] To assess the radiolabeling efficiency (R.E., %), the amount of radioactivity in the pellet and the supernatant after centrifugation were determined, and R.E. was calculated as the ratio between the amount of radioactivity in the pellet and total amount of radioactivity (pellet + supernatant).

To assess the radiochemical stability, NPs were prepared and purified as described above and subsequently resuspended in 200 μL of physiologic NaCl 0.9% solution (Braun Medical S.A.). The suspension was then divided into 3 different aliquots containing 50 μL of the NPs each. The aliquots were kept at 37 °C for 1, 3, and 12 h, respectively. The samples were then filtered (Amicon Ultra-15, 100 000 MWCO) and radioactivity was measured in a 2470 WIZARD2 Automate Gamma Counter (PerkinElmer). The dissociation of ^{18}F (expressed in percentage) at each time point was calculated as the ratio between the amount of radioactivity in the filtrate (decay-corrected) and the starting amount of radioactivity.

Animals. Healthy, 9−10-week-old Sprague−Dawley rats (Harlan, Udine, Italy) were used to examine the biodistribution pattern of radiolabeled NPs after intravenous injection. The animals were maintained and handled in accordance with the Guidelines for Accommodation and Care of Animals (European Convention for the Protection of Vertebrate Animals Used for Experimental and Other Scientific Purposes) and internal guidelines, and experimental procedures were approved by the local authorities. Rats were acclimated to the housing facility at 22−24 °C and 40−60% of humidity under light/dark conditions for at least 5 days prior to experiments.

In Vivo Biodistribution in Rats (PET-CT Imaging). Animals were anesthetized with 4.5% isoflurane in pure oxygen as carrier gas. ^{18}F-labeled NPs were suspended in a certain volume of saline solution (NaCl 0.9%) to obtain the required concentration of radioactivity (37−74 MBq/mL) and intravenously administered via one of the lateral tail veins. Formulations of ^{18}F-3P and ^{18}F-FBBA were also administered and used as controls.

PET-CT imaging was performed on an eXplore Vista-CT camera (GE Healthcare). Acquisition of the scans was started immediately after dose administration. Three beds were defined to acquire whole body images (frames: 4 × 4 min, 4 × 7 min, 4 × 20 min, 4 × 30 min; total acquisition time = 244 min). After acquisition, a CT scan was performed for later attenuation correction during image reconstruction. Random and scatter corrections were also applied to the reconstructed images (2DOSEM iterative algorithm, 4 iterations). PET-CT images were coregistered and analyzed using PMOD image processing tool. Volumes of interest (VOIs) were drawn in the kidneys, liver, stomach, and brain, using the CT images for anatomical reference. Time−activity curves (decay corrected) were obtained for each organ as cps/cm^3. Curves were transformed

DOI: 10.1021/acs.bioconjchem.5b00040
Bioconjugate Chem. 2015, 26, 582−592

into real activity (Bq/cm^3) curves by using a calibration factor. Injected dose and organ mass normalizations were finally applied to data to achieve percentage of injected dose per gram of tissue (%ID/g).

■ ASSOCIATED CONTENT

Supporting Information

Radiochemical conversions of [^{18}F]FBBA into [^{18}F]FBBA-PEG-thiol-acid (MW = 458.6 and 3300 Da) as a function of time and temperature, HPLC chromatograms, MS spectrum, MALDI-TOF-MS spectrum of [^{18}F]FBBA-PEG-thiol-acids, radiochemical conversion of [^{18}F]FBBA into [^{18}F]P and [^{18}F]3P as a function of time and temperature (Figure S1−S7). This material is available free of charge via the Internet at http://pubs.acs.org.

■ AUTHOR INFORMATION

Corresponding Authors

*E-mail: jllop@cicbiomagune.es.

*E-mail: salvador.borros@iqs.url.edu.

Notes

The authors declare no competing financial interest.

■ ACKNOWLEDGMENTS

The authors would like to thank GEMAT group of IQS for preliminary synthesis work, Sagetis-Biotech for promoting the investigation, Mikel González and Mikel Errasti for radioisotope production and radiochemical synthesis, Maria Puigivila for technical assistance during in vivo experiments and image analysis, and Dr. Javier Calvo for assistance in mass spectrometry. The in vivo work was partially funded by Ministerio de Economía y Competitividad (Project reference MAT2013-48169-R).

■ ABBREVIATIONS

[^{18}F]FBBA, 4-[^{18}F]fluorobenzyl-2-bromoacetamide; UV, ultraviolet; PEG-thiol-acid, α-thio-ω-carboxy poly(ethylene glycol); RCC, radiochemical conversion; HPLC, high-performance liquid chromatography; UPLC, ultraperformance liquid chromatography; ESI, electrospray ionization; MS, mass spectroscopy; TOF, time-of-flight; THF, tetrahydrofuran; AcOH, acetic acid; PBS, phosphate buffer solution; MW, molecular weight; MWCO, molecular weight cutoff; PTX, paclitaxel; BBB blood-brain barrier; MPS, mononuclear phagocyte system; RES, reticuloendothelial system

■ REFERENCES

(1) Guerrero-Martínez, A., Barbosa, S., Pastoriza-Santos, I., and Liz-Marzan, L. M. (2011) Nanostars shine bright for you. Colloidal synthesis, properties and applications of branched metallic nanoparticles. *Curr. Opin. Colloid Interface Sci. 16*, 118−127.

(2) Grzelczak, M., Pérez-Juste, J., Mulvaney, P., and Liz-Marzan, L. M. (2008) Shape control in gold nanoparticle synthesis. *Chem. Soc. Rev. 37*, 1783−1791.

(3) Blasco, C., and Picó, Y. (2011) Determining nanomaterials in food. *TRAC-Trends Anal. Chem. 30*, 84.

(4) Zielecka, M., Bujnowska, E., Kępska, B., Wenda, M., and Piotrowska, M. (2011) Antimicrobial additives for architectural paints and impregnates. *Prog. Org. Coatings 72* (1−2), 193−201.

(5) Stroyuk, A. L., Shvalagin, V. V., and Kuchmii, S. Y. (2005) Photochemical synthesis and optical properties of binary and ternary metal−semiconductor composites based on zinc oxide nanoparticles. *J. Photochem. Photobiol. A: Chem. 173* (2), 185−194.

(6) Blyszko, J., Kiernozycki, W., Guskos, N., Zolnierkiewicz, G., Typek, J., Narkiewicz, U., and Podsiadly, M. (2008) Study of mechanical properties of concrete with low concentration of magnetic nanoparticles. *J. Non-Cryst. Solids 354*, 4514−4518.

(7) Zhang, L., Gu, F. X., Chan, J. M., Wang, A. Z., Langer, R. S., and Farokhzad, O. C. (2008) Nanoparticles in Medicine: Therapeutic Applications and Developments. *Clin. Pharmacol. Ther. 83* (5), 761−769.

(8) Han, W., McCreary, K. M., Pi, K., Wang, W. H., Li, Y., Wen, H., Chen, J. R., and Kawakami, R. K. (2012) Spin transport and relaxation in graphene. *J. Magn. Magn. Mater. 324* (4), 369−381.

(9) Zhua, S.-C., Kai-Lun Yaoa, B., Gaoa, G.-Y., and Nia, Y. (2013) Spin-dependent transport in graphene nanoribbons adsorbed with vanadium in different positions. *Solid State Commun. 155*, 40−44.

(10) Basu, S., and Bhattacharyya, P. (2012) Recent developments on graphene and graphene oxide based solid state gas sensors. *Sens. Actuators, B: Chem. 173*, 1−21.

(11) Cui, L., Pu, T., Liu, Y., and He, X. (2013) Layer-by-layer construction of graphene/cobalt phthalocyanine composite film on activated GCE for application as a nitrite sensor. *Electrochim. Acta 88*, 559−564.

(12) Janib, S. M., Moses, A. S., and MacKay, J. A. (2010) Imaging and drug delivery using theranostic nanoparticles. *Adv. Drug Delivery Rev. 62* (11), 1052−1063.

(13) Shenoy, D. B., and Amiji, M. M. (2005) Poly(ethylene oxide)-modified poly(epsilon-caprolactone) nanoparticles for targeted delivery of tamoxifen in breast cancer. *Int. J. Pharm. 293* (1−2), 261−70.

(14) Chan, J. M., Valencia, P. M., Zhang, L., Langer, R., and Farokhzad, O. C. (2010) Polymeric nanoparticles for drug delivery. *Methods Mol. Biol. 624*, 163−175.

(15) Owens, D. E., and Peppas, N. A. (2006) Opsonization, biodistribution, and pharmacokinetics of polymeric nanoparticles. *Int. J. Pharm. 307* (1), 93−102.

(16) Moghimi, S. M., Hunter, A. C, and Murray, J. C. (2001) Long-circulating and target-specific nanoparticles: theory to practice. *Pharmacol. Rev. 53* (2), 283−318.

(17) Maeda, H. (2001) The enhanced permeability and retention (EPR) effect in tumor vasculature: the key role of tumor-selective macromolecular drug targeting. *Adv. Enzyme Regul. 41* (1), 189−207.

(18) Duncan, R. (2005) Targeting and intracellular delivery of drugs. In *Encyclopedia of Molecular Cell Biology and Molecular Medicine*, 2nd ed., pp 163−203, Wiley-VCH.

(19) Reiner, T., Keliher, E. J., Earley, S., Marinelli, B., and Weissleder, R. (2011) Synthesis and in vivo imaging of a 18F-labeled PARP1 inhibitor using a chemically orthogonal scavenger-assisted high-performance method. *Angew. Chem., Int. Ed. 50* (8), 1922−5.

(20) Locatelli, E., Gil, L., Israel, L. L., Passoni, L., Naddaka, M., Pucci, A., Reese, T., Gomez-vallejo, V., Milani, P., and Matteoli, M. (2012) Biocompatible nanocomposite for PET/MRI hybrid imaging. *Dove medical press*, 6021−6033 DOI: 10.2147/IJN.S38107.

(21) Nahrendorf, M., Zhang, H., Hembrador, S., Panizzi, P., Sosnovik, D. E., Aikawa, E., Libby, P., Swirski, F. K., and Weissleder, R. (2008) Nanoparticle PET-CT imaging of macrophages in inflammatory atherosclerosis. *Circulation 117* (3), 379−87.

(22) Devaraj, N. K., Keliher, E. J., Thurber, G. M., Nahrendorf, M., and Weissleder, R. (2009) 18F labeled nanoparticles for in vivo PET-CT imaging. *Bioconjugate Chem. 20* (2), 397−401.

(23) Guerrero, S., Herance, J. R., Rojas, S., Mena, J. F., Gispert, J. D., Acosta, G a, Albericio, F., and Kogan, M. J. (2012) Synthesis and in vivo evaluation of the biodistribution of a 18F-labeled conjugate gold-nanoparticle-peptide with potential biomedical application. *Bioconjugate Chem. 23* (3), 399−408.

(24) Rojas, S., Gispert, J. D., Martin, R., Abad, S., Menchon, C., Pareto, D., Victor, V. M., Alvaro, M., Garcia, H., and Herance, J. R. (2011) Biodistribution of amino-functionalized diamond nanoparticles. In vivo studies based on ^{18}F radionuclide emission. *ACS Nano* No. 7, 5552−5559.

DOI: 10.1021/acs.bioconjchem.5b00040
Bioconjugate Chem. 2015, 26, 582−592

(25) Di Mauro, P. P., and Borrós, S. (2014) Development of high drug loaded and customizing novel nanoparticles for modulated and controlled release of Paclitaxel. *Pharm. Res. 31* (12), 3461−77.
(26) Kuhnast, B., Klussmann, S., Hinnen, F., Boisgard, R., Rousseau, B., Frste, J. P., Tavitian, B., and Doll, F. (2003) Fluorine-18- and iodine-125-labelling of spiegelmers. *J. Labelled Compd. Radiopharm. 46* (13), 1205−1219.
(27) Koslowsky, I., Mercer, J., and Wuest, F. (2010) Synthesis and application of 4-[(18)F]fluorobenzylamine: A versatile building block for the preparation of PET radiotracers. *Org. Biomol. Chem. 8* (20), 4730−5.
(28) Herth, M. M., Barz, M., Moderegger, D., Allmeroth, M., Jahn, M., Thews, O., Zentel, R., and Ro, F. (2009) Radioactive labeling of defined HPMA-based polymeric structures using [18 F] FETos for in vivo imaging by positron emission tomography. *Biomacromolecules 10*, 1697−1703.
(29) Allmeroth, M., Moderegger, D., Gu, D., Koynov, K., Buchholz, H., Mohr, K., Ro, F., Zentel, R., and Thews, O. (2013) HPMA-LMA copolymer drug carriers in oncology: an in vivo PET study to assess the tumor line-specific polymer uptake and body distribution. *Biomacromolecules 14*, 3091−3101.
(30) Allmeroth, M., Moderegger, D., Biesalski, B., Koynov, K., Rösch, F., Thews, O., and Zentel, R. (2011) Modifying the body distribution of HPMA-based copolymers by molecular weight and aggregate formation. *Biomacromolecules 12* (7), 2841−9.
(31) Demeule, M., Currie, J.-C., Bertrand, Y., Ché, C., Nguyen, T., Régina, A., Gabathuler, R., Castaigne, J.-P., and Béliveau, R. (2008) Involvement of the low-density lipoprotein receptor-related protein in the transcytosis of the brain delivery vector angiopep-2. *J. Neurochem. 106* (4), 1534−44.
(32) Chen, X., Park, R., Shahinian, A. H., Bading, J. R., and Conti, P. S. (2004) Pharmacokinetics and tumor retention of 125I-labeled RGD peptide are improved by PEGylation. *Nucl. Med. Biol. 31* (1), 11−19.
(33) Wu, Z., Li, Z.-B., Cai, W., He, L., Chin, F. T., Li, F., and Chen, X. (2007) 18F-labeled mini-PEG spacered RGD dimer (18F-FPRGD2): synthesis and microPET imaging of alphavbeta3 integrin expression. *Eur. J. Nucl. Med. Mol. Imaging 34* (11), 1823−31.
(34) Stockhofe, K., Postema, J. M., Schieferstein, H., and Ross, T. L. (2014) Radiolabeling of nanoparticles and polymers for PET imaging. *Pharmaceuticals (Basel) 7* (4), 392−418.
(35) Ku, B., Terrazzino, S., Rousseau, B., Loc, C., Doignon, I., Pillon, F., David, C., Crouzel, C., and Tavitian, B. (2000) General method to label antisense oligonucleotides with radioactive halogens for pharmacological and imaging studies. *Bioconjugate Chem. 11* (5), 627−636.

DOI: 10.1021/acs.bioconjchem.5b00040
Bioconjugate Chem. 2015, 26, 582−592